Mechanisms of Signal Transduction:

Aberrant Localization of Intracellular Organelles, Ca^{2+} Signaling, and Exocytosis in Mist1 Null Mice

Xiang Luo, Dong Min Shin, Xinhua Wang,
Stephen F. Konieczny and Shmuel Muallem

J. Biol. Chem. 2005, 280:12668-12675.
doi: 10.1074/jbc.M411973200 originally published online January 21, 2005

THE JOURNAL OF BIOLOGICAL CHEMISTRY
Vol. 280, No. 13, Issue of April 1, pp. 12668–12675, 2005
Printed in U.S.A.

Aberrant Localization of Intracellular Organelles, Ca^{2+} Signaling, and Exocytosis in Mist1 Null Mice*

Received for publication, October 21, 2004, and in revised form, January 20, 2005
Published, JBC Papers in Press, January 21, 2005, DOI 10.1074/jbc.M411973200

Xiang Luo‡§, Dong Min Shin§¶, Xinhua Wang‡, Stephen F. Konieczny‖, and Shmuel Muallem‡**

From the ‡Department of Physiology, University of Texas Southwestern Medical Center at Dallas, Dallas, Texas 75390-9040, the ¶Department of Oral Biology, Research Center for Orofacial Hard Tissue Regeneration, Brain Korea 21 Project for Medical Science, Yonsei University College of Dentistry, Seoul 120-752, Korea, and the ‖Department of Biological Sciences and the Purdue Cancer Center, Purdue University, West Lafayette, Indiana 47907-2064

Ca^{2+} signaling and exocytosis are highly polarized functions of pancreatic acinar cells. The role of cellular architecture in these activities and the capacity of animals to tolerate aberrant acinar cell function are not known. A key regulator of acinar cell polarity is Mist1, a basic helix-loop-helix transcription factor. Ca^{2+} signaling and amylase release were examined in pancreatic acini of wild type and Mist1 null mice to gain insight into the importance of cellular architecture for Ca^{2+} signaling and regulated exocytosis. Mist1$^{-/-}$ acinar cells exhibited dramatically altered Ca^{2+} signaling with up-regulation of the cholecystokinin receptor but minimal effect upon expression of the M3 receptor. However, stimulation of inositol 1,4,5-trisphosphate production by cholecystokinin and carbachol was inefficient in Mist1$^{-/-}$ cells. Although agonist stimulation of Mist1$^{-/-}$ cells evoked a Ca^{2+} signal, often the Ca^{2+} increase was not in the form of typical Ca^{2+} oscillations but rather in the form of a peak/plateau-type response. Mist1$^{-/-}$ cells also displayed distorted apical-to-basal Ca^{2+} waves. The aberrant Ca^{2+} signaling was associated with mislocalization and reduced Ca^{2+} uptake by the mitochondria of stimulated Mist1$^{-/-}$ cells. Deletion of *Mist1* also led to mislocalization of the Golgi apparatus and markedly reduced digestive enzyme content. The combination of aberrant Ca^{2+} signaling and reduced digestive enzyme content resulted in poor secretion of digestive enzymes. Yet, food consumption and growth of Mist1$^{-/-}$ mice were normal for at least 32 weeks. These findings reveal that Mist1 is critical to normal organelle localization in exocrine cells and highlight the critical importance of maintaining cellular architecture and polarized localization of cellular organelles in generating a propagating apical-to-basal Ca^{2+} wave. The studies also reveal the spare capacity of the exocrine pancreas that allows normal growth and development in the face of compromised exocrine pancreatic function.

Ca^{2+} signaling regulates virtually all cell functions, including long term functions such as transcription and translation and short term functions such as neurotransmission and exocytosis (1, 2). In the pancreas, activation of Ca^{2+} signaling by G protein-coupled receptors (GPCRs)[1] plays a central role in digestive enzyme secretion (3). Abnormal enzyme secretion can lead to numerous diseases, including malnutrition in cystic fibrosis (4) and, more commonly, acute pancreatitis (5). Several studies have shown a strong association between aberrant Ca^{2+} signaling and pancreatitis (6–8). The polarized function of exocrine secretory cells requires polarized Ca^{2+} signaling. Indeed, stimulation of pancreatic acini GPCRs with physiological agonist concentrations triggers repetitive $[Ca^{2+}]_i$ oscillations in the form of Ca^{2+} waves that initiate at the apical pole and propagate to the basal pole (9–13).

The apical-to-basal Ca^{2+} waves are achieved by clustering Ca^{2+} signaling complexes at the apical pole (14–16). This leads to an apical-to-basal gradient of responsiveness, with the most responsive GPCR Ca^{2+} signaling complexes at the apical pole (16). In fact, functional mapping of Ca^{2+} signaling complexes has revealed that physiological Ca^{2+} signals are mostly triggered by the stimulation of Ca^{2+} signaling complexes at the apical pole (16). Once launched, the shape of the Ca^{2+} signals are regulated by many processes that affect the biochemical component of the Ca^{2+} signal that generates inositol 1,4,5-trisphosphate (IP_3) as well as the biophysical component that includes the Ca^{2+} release and influx channels and the sarco/endoplasmic reticulum ATPase (SERCA2b) and plasma membrane Ca^{2+} ATPase (PMCA) pumps (16).

Other important regulators of Ca^{2+} signaling in all cells (17), including pancreatic acinar (18, 19) and other secretory cells (20), are mitochondria. The seminal work of Rizzuto, Pozzan and co-workers showed that the mitochondria are in close proximity to the ER (21), thereby aligning the mitochondrial Ca^{2+} uptake pathway with the IP_3Rs to incorporate a large portion of the Ca^{2+} released from the ER (22, 23). Subsequently, mitochondria were shown to communicate with I_{crac} channels to regulate Ca^{2+} influx across the plasma membrane (24, 25). Mitochondrial localization in pancreatic acini is even more intricate. In these cells, three populations of energized mitochondria have been identified, namely a belt capping the secretory granules, a ring surrounding the nucleus, and a string lining the plasma membrane (19). The belt capping the secre-

* This work was supported by National Institutes of Health Grants DK38938 and DE13902 (to S. M.), Medical Science and Engineering Research Program of the Korea Science and Engineering Foundation Grant R13-2003-13 (to D. M. S.), and National Institutes of Health Grant DK55489 as well as funding from the Purdue Cancer Center (to S. F. K.). The costs of publication of this article were defrayed in part by the payment of page charges. This article must therefore be hereby marked "*advertisement*" in accordance with 18 U.S.C. Section 1734 solely to indicate this fact.

§ These authors contributed equally to this work and should be considered first co-authors.

** To whom correspondence should be addressed: University of Texas Southwestern Medical Center at Dallas, 5323 Harry Hines Blvd., Dallas, TX 75390-9040. Tel.: 214-648-2593; Fax: 214-648-2974; E-mail: SHMUEL.MUALLEM@utsouthwestern.edu.

[1] The abbreviations used are: GPCR, G proteins coupled receptor; CCK, cholecystokinin; CCKR, cholecystokinin; ER, endoplasmic reticulum; IP_3, inositol 1,4,5-trisphosphate; IP_3R, IP_3 receptor; M3R, M3 muscarinic receptor; PMCA, plasma membrane Ca^{2+} ATPase pump; RT, reverse transcription; SERCA2b, sarco/endoplasmic reticulum Ca^{2+} ATPase pump; TMRM, tetramethylrhodamine methyl ester; WT, wild type.

tory granules functions to confine Ca^{2+} signals to the apical pole at very low stimulus intensity (18), whereas the ring surrounding the nucleus isolates the nucleus from cytosolic Ca^{2+} tides (15, 19).

The intricate localization of Ca^{2+} signaling complexes and intracellular organelles is likely to be critical for the precise operation of the Ca^{2+} signaling apparatus and for regulated exocytosis in acinar cells. These assumptions can be directly examined only by testing the effect of perturbation of the cellular architecture on pancreatic acinar cell function. This has been a difficult problem to address but has now become possible with the availability of Mist1 null ($Mist1^{-/-}$) mice (26). Mist1 is a basic helix-loop-helix transcription factor that is essential for the normal development of serous acinar cells in various secretory glands, including the pancreas and salivary glands (26–30). Deletion of the *Mist1* gene (26, 30) or inhibition of Mist1 function (28, 29) leads to severe distortion of acinar cellular architecture, including loss of gap junctions and intercellular communication (28, 30), disorder of secretory granules (26–30), and acinar-to-ductal metaplasia (29). Additional changes in $Mist1^{-/-}$ cells include up-regulation of mRNA coding for the cholecystokinin (CCK) receptors and down-regulation of expression of IP_3R3 (26). However, the effect of distorted cellular architecture on Ca^{2+} signaling, pancreatic function, and animal growth and development has not been examined. In the present work we show that the Ca^{2+} signaling machinery in $Mist1^{-/-}$ cells is dramatically altered, resulting in aberrant agonist-evoked Ca^{2+} oscillations and Ca^{2+} waves. The altered Ca^{2+} response is not due to mislocalization of the remaining IP_3 receptors but rather is a consequence of mislocalization and aberrant Ca^{2+} uptake into mitochondria. The Golgi apparatus of $Mist1^{-/-}$ cells is diffuse and fragmented, which may explain the markedly decreased digestive enzyme content in the secretory granules. Exocytosis by $Mist1^{-/-}$ acinar clusters is undetectable at physiological agonist concentrations and is greatly reduced at pharmacological agonist concentrations. Remarkably, food consumption and weight gain remain similar for WT and $Mist1^{-/-}$ mice. These findings provide experimental evidence for the importance of cellular architecture in the generation and propagation of Ca^{2+} signals and illustrate the spare capacity of the exocrine pancreas to allow normal growth at reduced exocytosis.

EXPERIMENTAL PROCEDURES

Materials—Carbachol, CCK, and phorbol 12-myristate 13-acetate were purchased from Sigma. IP_3 was from Alexis. Fura2/AM, MitoTracker Green, Rhod-2, and Fluo-3 were from Teff Labs. Tetramethylrhodamine methyl ester (TMRM) was from Molecular Probes. Dr. Akihiko Tanimura (University of Hokkaido, Japan) generously provided anti-IP_3R1, IP_3R2, and IP_3R3 polyclonal antibodies. Anti-PMCA mAb 5F10 was purchased from Affinity Bioreagents. Anti-mannosidase II polyclonal antibodies were obtained from the University of Georgia. The polyclonal antibody against SERCA2b was provided by Dr. Frank Wuytack (University of Leuven, Belgium). Anti-M3 receptors antibodies were from US Biological.

Experimental Animals, Body Weights, and Food Intake—$Mist1^{-/-}$ mice were generated as described previously (26). All animals were housed in the animal care facility, and all protocols were approved by the University of Texas Medical Center at Dallas Animal Care Committee and conducted in accordance with the National Institutes of Health Guide for the Care and Use of Laboratory Animals. WT and $Mist1^{-/-}$ mice were housed individually. Food intake was measured three times per week using an Ohaus portable electronic scale with a sensitivity of 0.1 g. The body weight of litter mates was measured on the day of birth and then at 1-week intervals.

Preparation of Pancreatic Acini—Pancreatic acini and small acinar clusters were prepared by collagenase digestion as detailed previously (31). After isolation, the cells were suspended in solution A (140 mM NaCl, 5 mM KCl, 1 mM $MgCl_2$, 1 mM $CaCl_2$, 10 mM HEPES (pH 7.4 with NaOH), 10 mM glucose, 0.1% mM bovine serum albumin, and 0.02% soybean trypsin inhibitor) and kept on ice until used.

$[Ca^{2+}]i$ Imaging—Pancreatic acinar cells were loaded with Fura2, and $[Ca^{2+}]_i$ was imaged as described (32). In brief, to measure the dose response for agonists the Fura2 fluorescence ratio was measured at excitation wavelengths of 350 and 380 nm, and the ratio was calibrated to obtain $[Ca^{2+}]_i$. Ca^{2+} waves were recorded using a single excitation wavelength of 380 nm. The image of resting cells was acquired and taken as the fluorescence signal at time 0 (F_0). All subsequent images were divided by this image, and the traces and images are the calculated F_t/F_0, where F_t is the fluorescence at time t.

Simultaneous Measurement of Cytosolic and Mitochondrial Ca^{2+}—Rhod-2 and Fluo-3 were used for the measurement of mitochondrial and cytosolic Ca^{2+} signals, respectively. Loading with Rhod-2 was achieved by incubating acini is solution A with 8 μM Rhod-2/AM at 4 °C for 15 min. The acini were washed by centrifugation for 2 min at 30 × g to remove excess dye and then resuspended in solution A. The acini were incubated at room temperature for 30 min to hydrolyze the trapped Rhod-2. During this incubation, the acinar suspension was supplemented with 4 μM Fluo-3/AM. Finally, the acini were washed with solution A and kept on ice until use. Dye-loaded cells were transferred to a perfusion chamber, and Fluo-3 and Rhod-2 fluorescence was measured with a confocal laser-scanning system from Bio-Rad (MRC-1024) using the 488- and 568-nm lines, respectively. Laser intensity was reduced to 1–3% with neutral density filters to reduce photo bleaching. Images were recorded at a frequency of 1 Hz. The images were analyzed using MetaMorph software.

Mitochondrial Membrane Potential—Mitochondrial membrane potential was estimated from the incorporation of the potential-sensitive dye TMRM. Preliminary experiments showed that when monitored continuously, even at 1 μM the extent of TMRM incorporation was proportional to the mitochondrial membrane potential. TMRM uptake was measured by continuously perfusing acinar cells with a solution containing 1 μM TMRM. Once a plateau was reached, the acini were perfused with dye-free medium and then with medium containing 10 μM carbonyl cyanide *p*-(trifluoromethoxy)phenylhydrazone. TMRM fluorescence was recorded with the 488-nm line of the Bio-Rad MRC-1024 confocal microscope.

Measurement of IP_3—IP_3 levels were measured by a radioligand assay as described elsewhere (33). Acini suspended in solution A and incubated at 37 °C were stimulated with the indicated CCK or carbachol concentrations for 5–15 s, depending on agonist concentration. The reactions were stopped by the addition of perchloric acid, vigorous mixing, and incubation on ice for at least 10 min to allow precipitation of proteins. The supernatants were collected and transferred to clean tubes. Standards of IP_3 were prepared in the same manner. The perchloric acid was removed and IP_3 extracted by the addition of 0.15 ml of Freon and 0.15 ml of tri-*n*-octylamine. IP_3 content in the aqueous phase was measured by displacement of $[^3H]IP_3$ using microsomes prepared from bovine brain cerebella.

RT-PCR Analysis of CCK and M3 Receptors Expression—Acinar cell digests were placed in a Petri dish, and small clusters consisting of 3–5 cells were collected with a Pasteur pipette under microscopic examination to ensure lack of contamination with other cell types. The RNA was extracted from the acinar cells and brains of WT and $Mist1^{-/-}$ mice with TRIzol reagent (Invitrogen) and dissolved in diethyl pyrocarbonate-treated water. RT-PCR was performed using the same amount of RNA isolated from three WT and three $Mist1^{-/-}$ mice. The RT reaction was performed with the SuperScript™ II RT kit (Invitrogen) in a 20-μl reaction volume as suggested by the manufacturer. PCR primers were designed using Primer 3 version 0.2 and alignment by NCBI BLAST software. The primer sequences used were as follows: CCKA receptor sense, 5′-TCAGTGACCTCATGCTTTGC-3′, and CCKA receptor antisense, 5′-ATGAGTCCGTAAGCCACCAC-3′ (size of PCR product, 442 bp); muscarinic receptor 3 sense, 5′-TGCTGGTGATCAGCTTGAC-3′, and muscarinic receptor 3 antisense, 5′-TTCGTGCCTTGCTGTTGTAG-3′ (size of PCR product, 427 bp); β-actin-sense, 5′-TGTTACCAACTGGGACGACA-3′, and β-actin antisense, 5′-TCTCAGCTGTGGTGAAG-3′ (size of PCR product, 392 bp). The PCR reaction was initiated by a 5-min hot start at 94 °C followed by 35 amplification cycles that consisted of 50 s of incubation at 94 °C, 1 min at 55 °C, and 1 min at 72 °C, extended by 10 min at 72 °C, and terminated by incubation at 4 °C. Preliminary experiments using different amounts of cDNA were used to determine the optimal conditions, and amplification of actin mRNA was used to calibrate between samples.

Immunoblotting—Brain microsomes were prepared by homogenizing brain tissue from WT and $Mist1^{-/-}$ mice in a buffer containing (pH 7.6 with KOH) 100 mM KCl, 20 mM Tris-base, 1 mM EDTA, 1 mM benzamidine, and 1 mM phenylmethylsulfonyl fluoride. The homogenate was centrifuged at 1000 × g for 10 min at 4 °C. The supernatant was

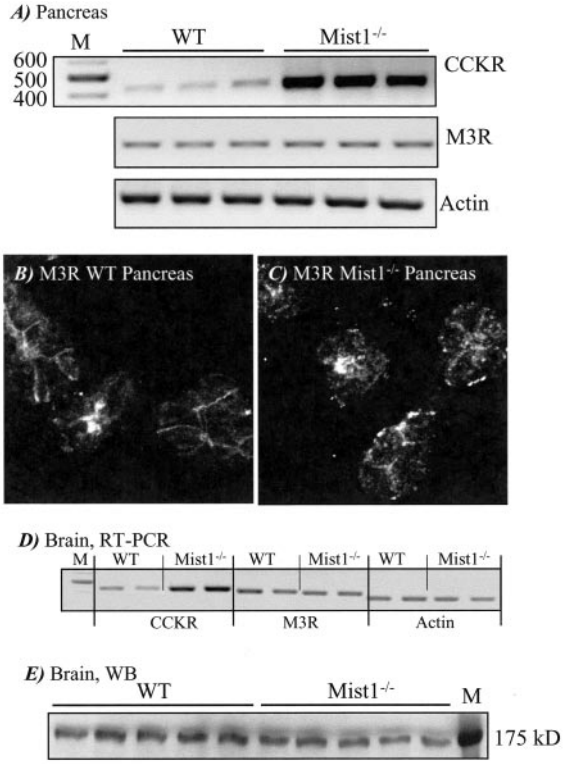

FIG. 1. **Expression of GPCRs in WT and $Mist1^{-/-}$ cells.** CCK receptor (*CCKR*), M3R, and actin mRNA levels were evaluated by RT-PCR using RNA isolated from pancreatic acinar cells (*A*) or brain (*D*) of WT and $Mist1^{-/-}$ mice. Frozen pancreatic sections of WT (*B*) and $Mist1^{-/-}$ mice (*C*) were used to immunolocalize the M3Rs. Brain extracts from 5 WT and 5 $Mist1^{-/-}$ mice were used to analyze expression of M3Rs by Western blot. *M*, molecular mass marker; *WB*, Western blot.

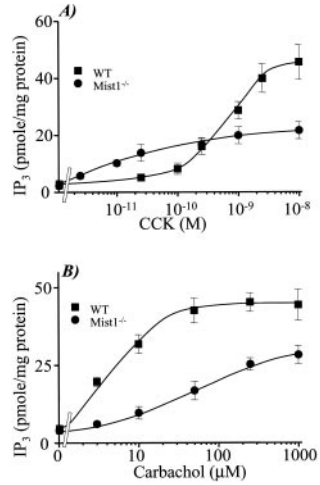

FIG. 2. **IP_3 production in WT and $Mist1^{-/-}$ cells.** For measurement of IP_3, pancreatic acini prepared from 2-month-old WT and $Mist1^{-/-}$ mice were stimulated with the indicated concentrations of CCK (*A*) or carbachol (*B*) for 5–10 s. IP_3 was extracted, and IP_3 content in the extract was measured by a radioligand assay as described under "Experimental Procedures."

collected and centrifuged at 40,000 × *g* for 30 min. The pellet was resuspended in homogenization buffer, and the microsomes were stored at −80 °C until use. The microsomes were extracted by a 1-h incubation on ice with a buffer containing 50 mM Tris (pH 6.8 with HCl), 150 mM NaCl, 2 mM EDTA, 2 mM EGTA and 0.5% Triton X-100 supplemented with protease inhibitors (0.2 mM phenylmethylsulfonyl fluoride, 10 μg/ml leupeptin, 15 μg/ml aprotinin, and 1 mM benzamidine). Released proteins were separated by SDS-PAGE and transferred to 0.2-μm polyvinylidene difluoride membranes, and the membranes were then blocked by a 1-h incubation at room temperature in 5% nonfat dry milk in TTBS solution containing 20 mM Tris-HCl, pH 7.5, 150 mM NaCl, and 0.05% Tween 20. The IP_3R1, IP_3R2, IP_3R3, PMCA, SERCA2b, and M3 receptors were detected by a 1–2-h incubation of individual membranes with the respective antibodies diluted in TTBS.

Immunocytochemistry—Immunostaning was performed as detailed previously (31, 32). Frozen pancreatic sections were fixed and permeabilized with 0.5 ml of cold methanol for 10 min at −20 °C. The sections were washed with phosphate-buffered saline alone and phosphate-buffered saline containing 50 mM glycine, and the nonspecific sites were blocked by a 1-h incubation with PBS containing 5% goat serum, 1% bovine serum albumin, and 0.1% gelatin. The medium was aspirated and replaced with 50 μl of blocking medium containing control serum or a 1:10 dilution of antibodies against the M3 muscarinic receptor (M3R), IP_3R2, and IP_3R3 and a 1:1000 dilution of antibodies against mannosidase II. After incubation with the primary antibodies overnight at 4 °C and three washes with the incubation buffer, the antibodies were detected with goat anti-rabbit or anti-mouse IgG tagged with fluorescein or rhodamine. Images were collected with a Bio-Rad MRC 1024 confocal microscope.

Measurement of Amylase, Lipase, and Trypsin—Freshly isolated acini from one mouse were suspended in 50 ml (for amylase) or 15 ml (for lipase and trypsin) of solution A. To measure total enzyme activity, 1 ml of cell suspension was lysed by the addition of 1% Triton X-100 and centrifuged for 2 min at 2000 × *g* at 4 °C, and the supernatant was collected. A second sample was used to measure protein content. Enzyme activity was measured in parallel from WT and $Mist1^{-/-}$ mice. To reduce variation due to feeding schedule, the mice were fasted for 24 h before the preparation of acini, and the results are expressed as the ratio between the activities in WT/$Mist1^{-/-}$ cells. For the measurement of exocytosis, portions of the 1.5-ml cell suspension were transferred to vials containing agonists to give the desired final concentrations. After 30 min of incubation at 37 °C, samples were transferred to Eppendorf tubes, the supernatants were separated from the acini by centrifugation, and the amylase released to the medium was measured. In each experiment, samples of cells were lysed to measure the total amylase content, and exocytotic amylase release was calculated as a fraction of total amylase content.

Amylase activity was measured with a Phadebas kit (Pharmacia and Upjohn Diagnostics, catalog number 10-5380-33) as described previously (34). In brief, 10-μl samples were diluted into 200 μl of buffer containing 20 mM NaH_2PO_4, 20 mM Na_2HPO_4, 50 mM NaCl, and 0.02% NaN_3, pH 7.0. 20 μl of the diluted samples were mixed with 1 ml of blue starch (10 mg/ml) and incubated for 10 min at 37 °C with gentle shaking. The reaction was stopped by the addition of 250 μl of 2 M NaOH, the supernatant was cleared by 5 min of centrifugation at 14,000 rpm, and the absorbance was measured at a wavelength of 595 nm.

Lipase activity was measured using *para*-nitrophenyl palmitate as a substrate (35). Samples of 0.1 ml were added to 2.4 ml of a freshly prepared *para*-nitrophenyl palmitate solution (30 mg of *para*-nitrophenyl palmitate in 100 ml of 100 mM Tris buffer, pH 8.5, 207 mg of Na^+-deoxycholate, and 100 mg of gum arabic) and incubated for 1 h at 37 °C with gentle shaking. The reactions were terminated by the addition of 0.2 ml of 100 mM $CaCl_2$, the samples were centrifuged at 14,000 rpm for 2 min, and the absorbance was measured at a wavelength of 410 nm.

Trypsin activity was determined with the substrate *N*-α-benzoyl-arginine-*p*-nitroanilide as described previously (36) with a slight modification. Samples of 100 μl were added into 2.4 ml of 1 mM substrate *N*-α-benzoyl-arginine-*p*-nitroanilide dissolved in a solution containing 100 mM Tris, pH 9.0, and 10 mM $CaCl_2$ and incubated for 1 h at 37 °C. The reactions were stopped by addition of 5 μl of 0.5 mg/ml soybean trypsin inhibitor, and the change in absorbance at 410 nm was monitored.

Statistics—When appropriate, results are presented as the mean ± S.E. of the indicated number of experiments. Statistical significance was evaluated by a two-way analysis of variance. All immunostaining experiments were repeated at least five times with similar results.

RESULTS AND DISCUSSION

Impaired Stimulation of Ca^{2+} Signaling in $Mist1^{-/-}$ Cells—The up-regulation of the CCK receptor mRNA in $Mist1^{-/-}$ mouse pancreatic acinar cells (26) was confirmed by RT-PCR in pancreatic acinar cells (Fig. 1*A*). However, this increase was not observed for all GPCRs. Initial analysis by RT-PCR showed that expression of M3R mRNA in the pancreas of $Mist1^{-/-}$ mice was unchanged or slightly up-regulated (Fig. 1*A*). An attempt to quantitate the extent of protein expression of M3Rs

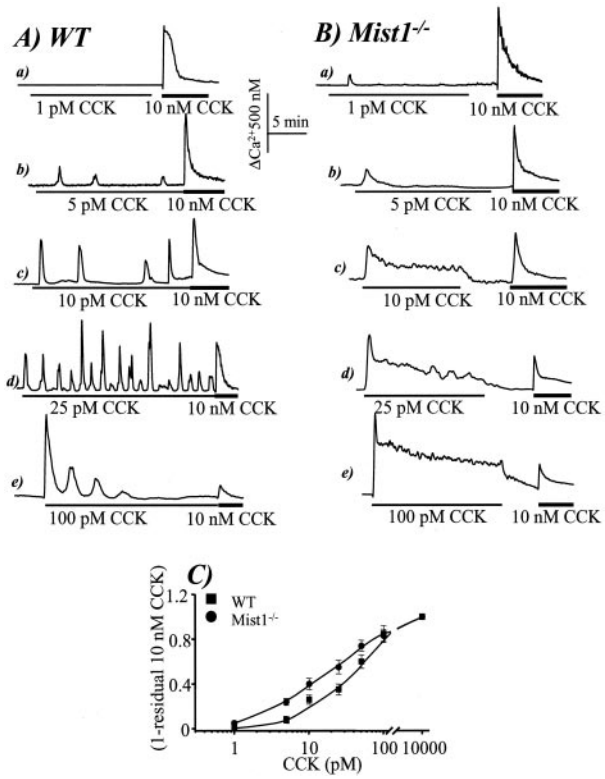

FIG. 3. **CCK-evoked Ca^{2+} signaling in WT and $Mist1^{-/-}$ cells.** WT (*A*) or $Mist1^{-/-}$ cells (*B*) loaded with Fura2 were stimulated with the indicated concentrations of CCK. At the end of each experiment the cells were stimulated with 10 nM CCK to discharge all remaining ER Ca^{2+}. The extent of stimulation at each CCK concentration was calculated from the reduction of the Ca^{2+} signal evoked by the maximal CCK concentration to determine the dose response for CCK stimulation (*C*) of WT (■) and $Mist1^{-/-}$ cells (●).

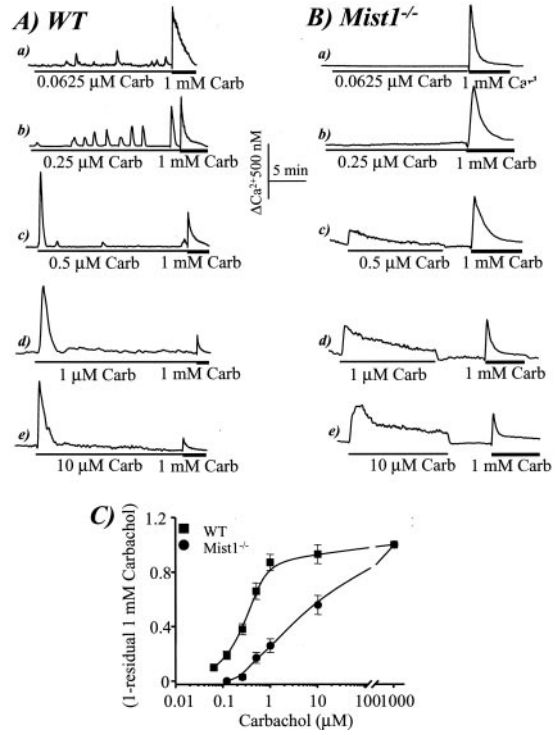

FIG. 4. **Carbachol-evoked Ca^{2+} signaling in WT and $Mist1^{-/-}$cells.** WT (*A*) or $Mist1^{-/-}$ cells (*B*) were stimulated with the indicated carbachol (*Carb*) concentrations. At the end of each experiment, the cells were stimulated with 1 mM carbachol to calculate the extent of cells stimulation at each carbachol concentration and determine the dose response for carbachol stimulation (*C*) of WT (■) and $Mist1^{-/-}$ cells (●).

by Western blot in pancreatic extracts failed because of poor signal/noise. However, the antibodies gave a reasonable signal in immunostaining. Fig. 1, *B* and *C*, show enrichment of M3R expression at the apical pool of cells from WT and $Mist1^{-/-}$ mice and comparable staining intensity. To further analyze receptor expression, we examined the expression of mRNA and protein in the brains of the mice. Fig. 1*D* shows that, similar to findings in the pancreas, brain mRNA for CCK receptors was up-regulated, and for M3Rs it was unchanged. Western blot analysis of extracts prepared from five brains of WT and five brains of $Mist1^{-/-}$ mice showed a small reduction in the level of M3Rs protein in $Mist1^{-/-}$ mice (18 ± 5%, $n = 5$) (Fig. 1*E*).

The aberrant localization of secretory granules, the reduction in expression of IP_3R3, and the up-regulation of CCK receptor mRNA in the $Mist1^{-/-}$ mouse pancreatic acini (26) raised the question of how Ca^{2+} signaling is affected in these cells. Measurement of IP_3 production showed that signaling by all GPCRs was impaired in $Mist1^{-/-}$ cells. Loss of the Mist1 protein reduced the EC_{50} for CCK stimulation from ~0.83 to 0.032 nM and reduced the maximal production of IP_3 by ~50% (Fig. 2*A*). $Mist1^{-/-}$ acinar cells showed an increased EC_{50} for carbachol from ~3.7 to 46 μM and a reduced maximal production of IP_3 of ~30% (Fig. 2*B*). The increased apparent affinity to CCK may relate to the increased mRNA levels of the CCK receptors (26) (Fig. 1*A*). The modest change in M3R mRNA and protein is consistent with this interpretation. However, the reduction in maximal IP_3 production indicates a generally impaired activation of G proteins by the M3R and an impaired activation of phospholipase Cβ by GPCRs.

The consequence of impaired IP_3 production on the pattern of Ca^{2+} signaling is shown in Figs. 3 and 4. *Panels A* and *B* in each figure show example traces from individual experiments, whereas the *panels C* (Figs. 3 and 4) summarize results from multiple experiments. CCK stimulated Ca^{2+} signaling with a higher affinity in $Mist1^{-/-}$ cells (Fig. 3*C*), whereas the affinity for carbachol to trigger a Ca^{2+} signal was lower in $Mist1^{-/-}$ cells (Fig. 4*C*), as was expected from their effects on IP_3 production. However, maximal concentrations of both agonists increased $[Ca^{2+}]_i$ to similar levels in WT and $Mist1^{-/-}$ cells (CCK, 723 ± 81 nM in WT and 744 ± 79 nM in $Mist1^{-/-}$; carbachol, 726 ± 88 nM in WT and 711 ± 63 nM in $Mist1^{-/-}$; n was >35 acini from 11 $Mist1^{-/-}$ and 11 age-matched WT mice, ages 2–11 months). A notable difference between WT and $Mist1^{-/-}$ cells was that often agonists did not induce $[Ca^{2+}]_i$ oscillations in the $Mist1^{-/-}$ cells but rather a single Ca^{2+} transient with a subsequent plateau (Figs. 3, *A* and *B* and 4, *A* and *B*).

The Ca^{2+} signal in pancreatic acinar cells occurs as a propagated Ca^{2+} wave (9–13). Therefore, we measured Ca^{2+} waves in WT and $Mist1^{-/-}$ cells. Stimulation of WT acini with low agonist concentrations such as 1 μM carbachol (not shown) or 10 pM CCK (Fig. 5*A*) resulted in a slowly propagating Ca^{2+} wave that was initiated at the apical pole. On the other hand, in multiple attempts it was almost impossible to resolve a Ca^{2+} wave at low agonist concentrations in $Mist1^{-/-}$ cells (for example, Fig. 5*B*). However, we noted that $[Ca^{2+}]_i$ increased faster in $Mist1^{-/-}$ cells. The Ca^{2+} waves in $Mist1^{-/-}$ cells could sometimes be resolved at intermediate agonist concentrations. Stimulation of heterozygous $Mist1^{+/-}$ cells (as well as WT cells) with 5 μM carbachol generated Ca^{2+} waves that propagated through the cell at a rate of 16.7 ± 0.5 μm/sec (Fig. 5*C*). Interestingly, although $Mist1^{-/-}$ cells also initiated a Ca^{2+} signal at the apical pole, even at the intermediate agonist concentrations it was not always possible to observe a clear Ca^{2+} wave for two main reasons (Fig. 5*B*). First, the Ca^{2+} wave

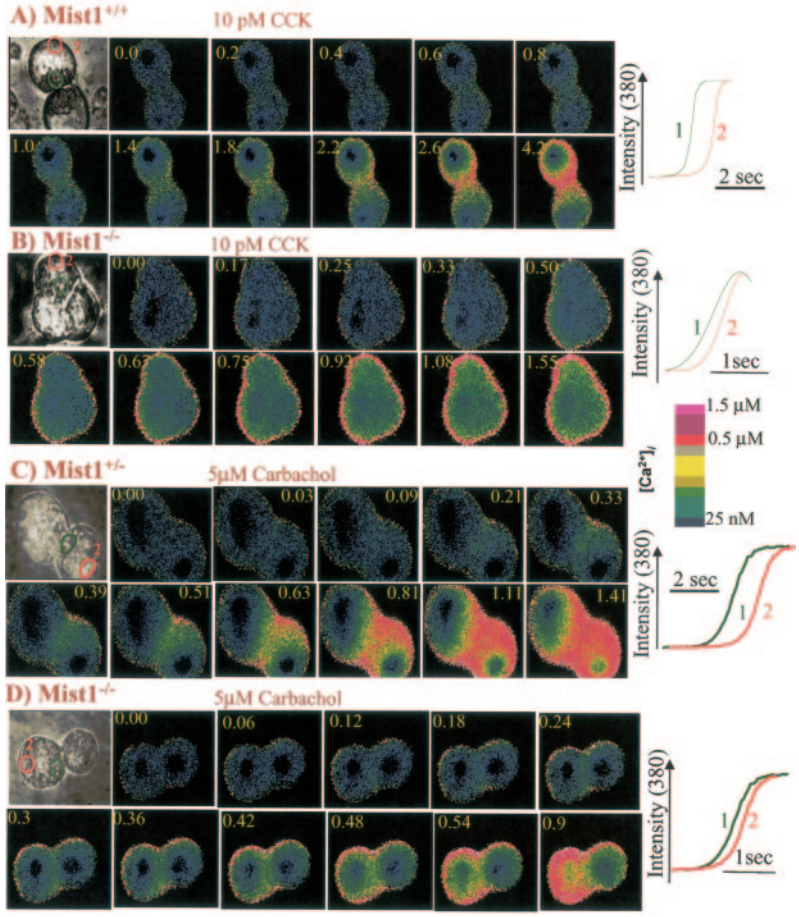

FIG. 5. **Ca2⁺ waves in Mist1$^{+/-}$ and Mist1$^{-/-}$ cells.** WT (*A*), Mist1$^{+/-}$ (*C*), and Mist1$^{-/-}$ cells (*B* and *D*) were stimulated with 10 pM CCK (*A* and *B*) or 5 μM carbachol (*C* and *D*) to better resolve the Ca^{2+} wave in Mist1$^{-/-}$ cells. In each *panel*, the first image is the bright field image that also indicates the apical (*green*) and basal pole (*red*) areas analyzed. The traces indicate the time course of the change in Fura2 fluorescence at the regions labeled in the bright field images. The fluorescence images depict the change in $[Ca^{2+}]_i$ at selective times during CCK or carbachol stimulation. The times in seconds at which the images were acquired are indicated by the *yellow numbers*.

in Mist1$^{-/-}$ cells propagated very rapidly. When it could be resolved, the Ca^{2+} wave propagated at a rate of 43.6 ± 5.8 (n = 14) μm/s. Second, the Ca^{2+} wave in Mist1$^{-/-}$ cells propagated along the cell periphery and only then proceeded concentrically toward the cell center (Fig. 5*D*). These results suggest that the proteins and organelles that control the propagation of the Ca^{2+} wave do not function properly in the Mist1$^{-/-}$ cells. This can be due to mislocalization of IP_3Rs that are concentrated at the apical pole of pancreatic acini (14, 15), mislocalization of the mitochondria that determine the pattern of the Ca^{2+} wave (18–20), or both.

Expression and Localization of Ca^{2+} Signaling Proteins—The Ca^{2+} waves in pancreatic acini are regulated by localization of IP_3 receptors (14, 15) and other Ca^{2+} signaling proteins (13, 16) and by Ca^{2+} uptake into the mitochondria (18–20). Our previous work has shown that the level of IP_3R3 is down-regulated in Mist1$^{-/-}$ cells (26). To test if the down-regulation of IP_3R3 is a more general phenomenon and whether deletion of the *Mist1* gene affects localization of Ca^{2+} signaling complexes, we analyzed the expression of individual IP_3Rs in brain extracts and the localization of IP_3R2 and IP_3R3 in pancreatic acini. The Western blot analysis in Fig. 6*A* shows that deletion of *Mist1* reduced expression of IP_3R3 in the brain by ~65 ± 11% (n = 5). On the other hand, expression of IP_3R1, IP_3R2, SERCA2b, and PMCA was not affected. This indicates that down-regulation of IP_3R3 expression in Mist1$^{-/-}$ mice is not specific to acinar cells, raising the possibility that loss of Mist1 may effect IP_3R3 expression in other cell types. The immunolocalization in Fig. 6*B* revealed a lack of IP_3R3 and completely normal localization of IP_3R2 in pancreatic acini of Mist1$^{-/-}$ cells.

The results in Fig. 6 indicate that the distorted Ca^{2+} signaling and Ca^{2+} waves observed in Mist1$^{-/-}$ cells are not due to a general aberrant expression of Ca^{2+} signaling proteins or to mislocalization of the remaining IP_3Rs. Furthermore these findings and those in Figs. 3 and 4 indicate that the function of IP_3R3, and perhaps other IP_3Rs, is cell-specific. A recent work provides strong evidence in cell lines that IP_3R1 is essential for receptor-triggered Ca^{2+} oscillations, whereas IP_3R3 functions as an anti-Ca^{2+} oscillatory unit (38). That is, knock-down of IP_3R3 by small interfering RNA enhanced Ca^{2+} oscillations. On the other hand, Ca^{2+} oscillations were rare in Mist1$^{-/-}$ cells, where the IP_3R3 is markedly down-regulated (Figs. 3 and 4). This would suggest a cell-specific function of IP_3R3.

Mitochondrial Localization and Function in Mist1$^{-/-}$ Cells—The Ca^{2+} waves in pancreatic acini and Ca^{2+} signaling in many cells are prominently regulated by Ca^{2+} uptake into the mitochondria (18–25). Therefore, we next compared localization and function of the mitochondria in WT and Mist1$^{-/-}$ cells. Localization of mitochondria was followed using Mito-Tracker Green detection, and mitochondrial and cytosolic Ca^{2+} levels were measured with Rhod-2 and Fluo-3, respectively. As expected, the energized mitochondria in WT cells were clustered around the secretory granules and the nucleus and next to the plasma membrane, but they were completely excluded from the secretory granule area in pancreatic acini (Fig. 7, *A*, *B*, and *E*) (19). By contrast, mitochondria in Mist1$^{-/-}$ acinar cells were highly disorganized (Fig. 7, C, *D*, and *F*). Energized mitochondria were found at all regions of the basal pole. In addition, although mostly excluded from the apical pole in Mist1$^{-/-}$ cells, some mitochondria could also be found at the periphery of the apical pole or sometimes within the apical pole itself.

Disorganization of the mitochondria in Mist1$^{-/-}$ cells resulted in the inhibition of Ca^{2+} uptake into the mitochondria when the cells were stimulated with low agonist concentrations. In WT cells, $[Ca^{2+}]_i$ and mitochondrial Ca^{2+} increases

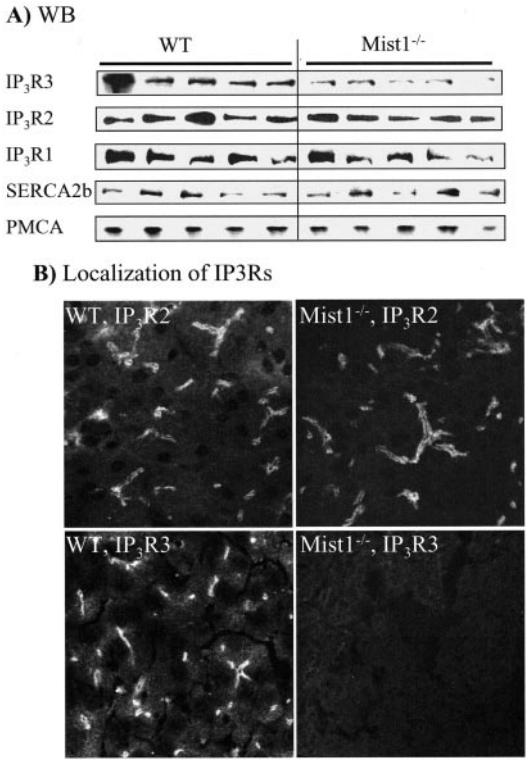

FIG. 6. **Expression of Ca^{2+} signaling proteins in WT and $Mist1^{-/-}$ cells.** *Panel A*, brain extracts from 5 WT and 5 $Mist1^{-/-}$ mice were used to analyze expression of IP_3R3, IP_3R2, IP_3R1, SERCA2b, and PMCA. *Panel B*, frozen pancreatic sections of WT and $Mist1^{-/-}$ mice were used to immunolocalize IP_3R2 and IP_3R3 as indicated.

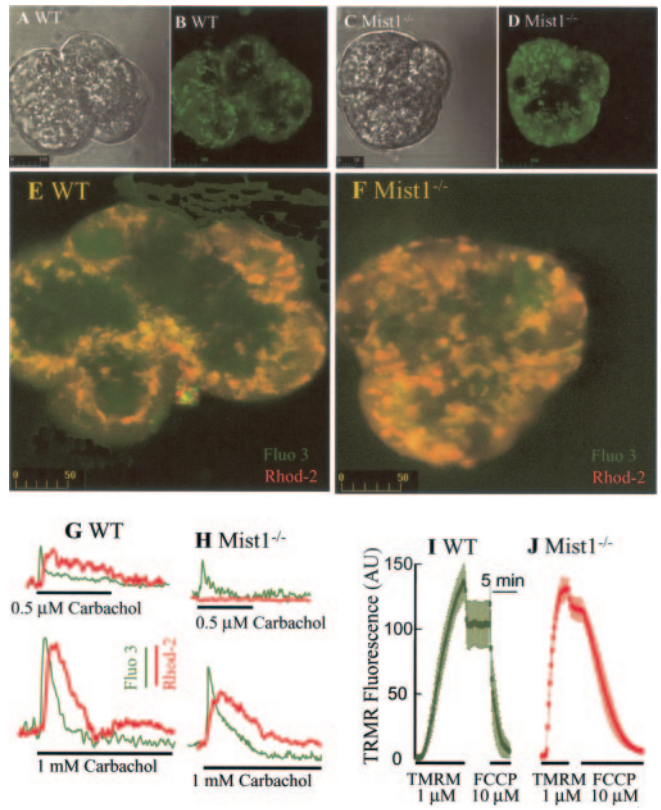

FIG. 7. **Mitochondrial and cytoplasmic Ca^{2+} in WT and $Mist1^{-/-}$ cells.** WT (*A* and *B*) and $Mist1^{-/-}$ acini (*C* and *D*) were loaded with MitoTracker Green by a 10-min incubation with solution A containing 1 μM MitoTracker Green and imaged by confocal microscopy. *Panels A* and *C* are the bright field images, and *panels B* and *D* are the corresponding fluorescence images. WT (*E* and *G*) and $Mist1^{-/-}$ (*F* and *H*) acini were loaded with Fluo3 (*green*) and Rhod-2 (*red*) to measure cytosolic and mitochondrial Ca^{2+}, respectively. The images show the Fluo3 and Rhod-2 fluorescence of resting cells. The cells were stimulated with 0.5 μM or 1 mM carbachol, and the fluorescence changes in the cytosol (*green traces*) and mitochondria (*red traces*) were analyzed and plotted as arbitrary changes in fluorescence after normalization to the same scale. Similar results were obtained in three separate cell preparations with at least 10 acini. WT (*I*) and $Mist1^{-/-}$ (*J*) acini were incubated with 1 μM TMRM for 5–7 min. The dye was then washed by perfusion, and the cells were exposed to 10 μM carbonyl cyanide *p*-(trifluoromethoxy)phenylhydrazone (*FCCP*). The results show the mean ± S.E. of 9–13 acini from two preparations.

were observed when the cells were stimulated with carbachol concentrations between 0.1 and 1 μM. By contrast, a $[Ca^{2+}]_i$ increase was observed at carbachol concentrations of 0.5 and 1 μM in $Mist1^{-/-}$ cells with no change in mitochondria Ca^{2+}. Fig. 7, *G* and *H* show the response to 0.5 μM carbachol. However, a normal increase in mitochondrial Ca^{2+} was observed at carbachol concentrations of >5 μM. The nearly normal increase in mitochondrial Ca^{2+} at intermediate agonist concentrations suggests that mislocalization of mitochondria rather than loss of mitochondrial membrane potential was the major reason for reduced Ca^{2+} uptake into the mitochondria at a low agonist concentration. This was verified directly by measuring the mitochondrial membrane potential with TMRM. Fig. 7, *I* and *J* show the similar TMRM uptake in WT and $Mist1^{-/-}$ cells, respectively.

Mitochondrial localization has a critical role in Ca^{2+} signaling. Previous work has emphasized the importance of the close apposition of the mitochondria to the ER for Ca^{2+} uptake into the mitochondria (22, 23), regulation of the I_{crac} Ca^{2+} influx channel (24, 25), and regulation of the Ca^{2+} wave in secretory cells (18–20). Furthermore, Ca^{2+} uptake into the mitochondria is essential for mitochondrial and cellular energy metabolism (39, 40). The disorganization of the mitochondria in $Mist1^{-/-}$ cells can explain the lack of Ca^{2+} uptake by the mitochondria when the cells are stimulated at a low agonist concentration. Such an uptake requires close communication between the mitochondria and the ER (21, 23). Because Ca^{2+} uptake by the mitochondria plays an important role in controlling the Ca^{2+} wave (18–20), the disorganization of mitochondria is likely responsible for the rapid spreading of Ca^{2+} from the apical to the basal pole and the concentric Ca^{2+} signal observed in $Mist1^{-/-}$ cells (Fig. 5).

Digestive Enzyme Content in $Mist1^{-/-}$ Cells—To determine the effect of deleting the *Mist1* gene on pancreatic exocrine function, it was necessary to first measure how the absence of the Mist1 protein affects digestive enzyme content. Examination of the ER and the Golgi apparatus, which govern protein synthesis, revealed that the overall ER structure remained normal in $Mist1^{-/-}$ cells (29). On the other hand, deletion of Mist1 modified the structure of the Golgi apparatus. Staining the Golgi with mannosidase II revealed a diffused Golgi organization in $Mist1^{-/-}$ cells (Fig. 8*A*). As expected, the diffused Golgi resulted in reduced digestive enzyme content in pancreatic acini. $Mist1^{-/-}$ cells contained 2.5–3-fold less amylase, trypsin, and lipase than WT cells (Fig. 8*B*). Amylase content measured in mice as young as 1 month and as old as 15 months were found to be similarly reduced, suggesting that reduction in digestive enzyme content does not develop with time but is a relatively early defect in $Mist1^{-/-}$ acinar cells. This observation is consistent with Mist1 controlling the transcriptional regulation of genes involved in the localization of several organelles, including the secretory granules, the mitochondria, and the Golgi apparatus in pancreatic acini, and possibly functioning as a master regulator of intracellular organelle localization. Further studies will be needed to establish this intriguing possibility.

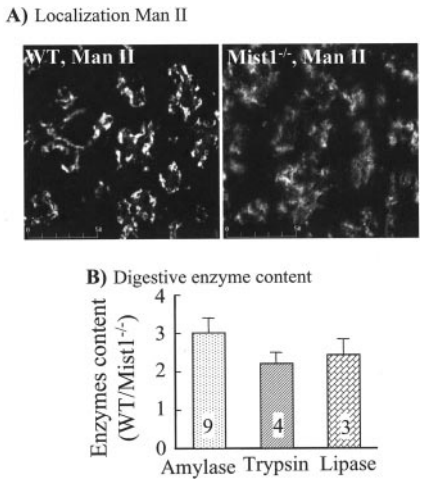

FIG. 8. **Localization of the Golgi apparatus and digestive enzyme content in WT and $Mist1^{-/-}$ cells.** *Panel A*, frozen pancreatic sections of WT and $Mist1^{-/-}$ mice were used to immunolocalize mannosidase II (*Man II*). *Panel B*, total extracts of pancreatic acini from WT and $Mist1^{-/-}$ mice were used to measure amylase, trypsin, and lipase activity. Digestive enzyme activities were calculated per milligram of protein and are expressed as the ratio of activities measured in WT and $Mist1^{-/-}$ acini. The number of determinations from separate pancreases is indicated in each column.

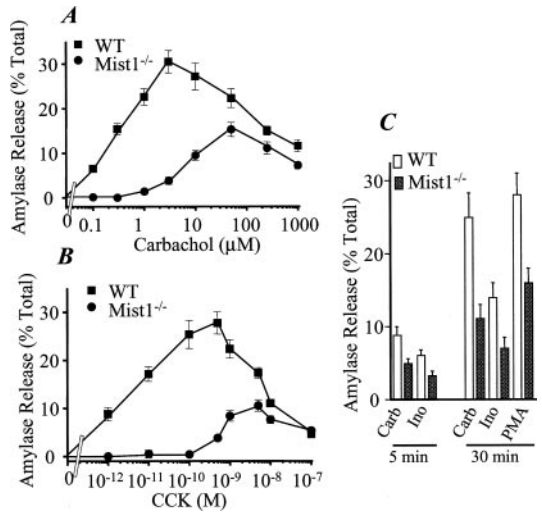

FIG. 9. **Exocytosis in WT and $Mist1^{-/-}$] cells.** WT (■) and $Mist1^{-/-}$ (●) acini were stimulated for 30 min with the indicated concentrations of carbachol (*A*) or CCK (*B*). In *panel C*, WT (*open columns*) and $Mist1^{-/-}$ acini (*dark columns*) were also stimulated with 10 μM carbachol (*Carb*), 5 μM ionomycin (*Ino*), or 1 μM phorbol 12-myristate 13-acetate (*PMA*) for 5 or 30 min. Amylase activity in the supernatant was measured and calculated as the percentage of total activity in each group of acini. The results are the mean ± S.E. of four (*A* and *B*) and three experiments (*C*).

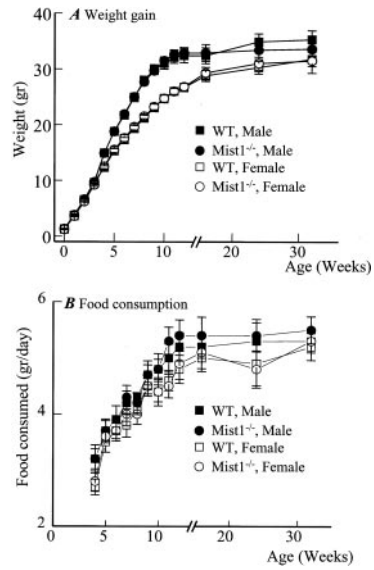

FIG. 10. **Weight gain and food consumption of WT and $Mist1^{-/-}$ cells.** Groups of eight WT male (■), WT female (□), $Mist1^{-/-}$ male (●), and $Mist1^{-/-}$ female (○) mice were kept with their mothers for 4 weeks. After 4 weeks, mice from each group were housed in two cages. Weight was determined on the day of birth and for the subsequent 32 weeks daily or weekly, as needed. Measurement of food consumption started after weaning. Weight (*A*) was averaged each week, and food consumption (*B*) per day was calculated from the weekly average. For the 16-, 24-, and 32-week time points, weight gain and food consumption were determined only for the week of interest. None of the values for any given week were statistically different between WT and $Mist1^{-/-}$ mice.

Exocytosis and Growth in $Mist1^{-/-}$ Mice—Changes in $[Ca^{2+}]_i$ are the primary stimulators of exocytosis in pancreatic acini (3), and aberrant Ca^{2+} signaling is intimately associated with pancreatitis (6–8). In addition, digestive enzyme content is low in $Mist1^{-/-}$ cells. Therefore, we expected that digestive enzyme secretion would be modified in $Mist1^{-/-}$ cells and that the $Mist1^{-/-}$ mice would show retarded growth or higher food consumption. Gross inspection of the pancreases of $Mist1^{-/-}$ mice did not reveal any major differences in the size or shape of the organ. However, the pancreas of $Mist1^{-/-}$ mice tended to be more fibrotic than that of WT mice, as suggested by the need for longer digestion by collagenase to liberate $Mist1^{-/-}$ acini (not shown). Large acinar clusters comprise of 8–30 cells prepared from WT and $Mist1^{-/-}$ mice were used to measure stimulated amylase secretion as a measure of exocytosis. In the large clusters, the structure of the acini and the stimulated enzyme secretion is preserved and faithfully reflects enzyme secretion *in vivo* (41). As shown in Fig. 9, exocytosis in response to both carbachol and CCK was markedly impaired in $Mist1^{-/-}$ acini. In fact, no exocytosis could be measured in $Mist1^{-/-}$ acini stimulated with physiological agonist concentrations. Low exocytosis in $Mist1^{-/-}$ acini was observed only at the very high agonist concentrations that are pathological in WT animals. Furthermore, after correction for total amylase content, the peak amylase release by $Mist1^{-/-}$ acini detected at the higher agonist concentrations was only 50% of that measured in WT acini. Because high agonist concentrations increase $[Ca^{2+}]_i$ to similar levels in WT and $Mist1^{-/-}$ cells (Figs. 3 and 4), this finding suggests that mislocalization of secretory granules contributed to the aberrant exocytosis. This was tested directly by measuring the response to increasing $[Ca^{2+}]_i$ with ionomycin and stimulating protein kinase C with phorbol 12-myristate 13-acetate. Fig. 9*C* shows that deletion of *Mist1* impaired exocytosis in response to both ionomycin and phorbol 12-myristate 13-acetate stimulation by ~40–50%. However, it is important to note that exocytosis stimulated by physiological agonist concentrations was impaired by 80–95%, indicating that impaired Ca^{2+} signaling was the major cause for the poor exocytosis in $Mist1^{-/-}$ cells.

An important implication of the findings in Fig. 9 is that the precise pattern of Ca^{2+} oscillations and waves are critical for exocytosis. Thus, CCK between 1 and 100 pM and carbachol at 0.5 and 1 μM evoked robust Ca^{2+} increases in $Mist1^{-/-}$ cells but did not stimulate any exocytosis. On the other hand, the same or lower agonist concentrations evoked a smaller Ca^{2+} signal but markedly stimulated exocytosis in WT acini. The only difference in the Ca^{2+} signals in WT and $Mist1^{-/-}$ cells is that in WT cells the agonists induced repetitive Ca^{2+} oscillations and propagated Ca^{2+} waves.

The impaired stimulated exocytosis was expected to lead to

malnutrition, retarded growth, and/or increased food consumption in the Mist1$^{-/-}$ mice. Remarkably, this was not the case for male or female Mist1$^{-/-}$ mice (Fig. 10, *A* and *B*). Food consumption and growth were similar in WT and Mist1$^{-/-}$ mice for the 32 weeks that the data were recorded. This was the case during both the rapid (first 10 weeks) and slow growth (weeks 11–32) phases of the animals development. These results suggest that either secretion *in vivo* was affected less than what was observed with isolated acinar clusters or that the residual pancreatic function in Mist1$^{-/-}$ mice is sufficient to support the food digestion and nutritional requirement of these animals.

In conclusion, the findings of the present work reveal several new roles for Mist1. We have extended previous studies to show that Mist1 controls the localization and perhaps the integrity of the mitochondria and the Golgi apparatus in addition to regulating the localization of secretory granules. The disordered localization of intracellular organelles leads to aberrant Ca^{2+} signaling that prevents Ca^{2+} oscillations and distorts the apical-to-basal Ca^{2+} waves. These findings provide evidence for the importance of cellular architecture in the generation and propagation of the Ca^{2+} signals. The aberrant Ca^{2+} signaling and cell architecture also result in greatly reduced exocytosis, further demonstrating the importance of Ca^{2+} signaling in exocrine pancreatic function. The unexpected finding is the lack of any effect of the compromised acinar pancreatic function on food consumption and animal growth. Whether this is the result of a less compromised pancreatic function *in vivo* or the large spare capacity of the pancreatic function remains to be determined. However, given the known spare capacity of the pancreas and the fact that secretion by acinar clusters accurately reflects secretion *in vivo* (41), it is likely that the spare pancreatic function protected the Mist1$^{-/-}$ animals to allow normal growth with no need for increased food consumption.

REFERENCES

1. Berridge, M. J., Bootman, M. D., and Roderick, H. L. (2003) *Nat. Rev. Mol. Cell. Biol.* **4,** 517–529
2. Carafoli, E. (2002) *Proc. Natl. Acad. Sci. U. S. A.* **99,** 1115–1122
3. Williams, J. A. (2001) *Ann. Rev. Physiol.* **63,** 77–97
4. Hankard, R., Munck, A., and Navarro, J. (2002) *Horm. Res.* **58,** Suppl. 1, 16–20
5. Saluja, A. K., Bhagat, L., Lee, H. S., Bhatia, M., Frossard, J. L., and Steer, M. L. (1999) *Am. J. Physiol.* **276,** G835–G842
6. Kim, J. Y., Kim, K. H., Lee, J. A., Namkung, W., Sun, A. Q., Ananthanarayanan, M., Suchy, F. J., Shin, D. M., Muallem, S., and Lee, M. G. (2002) *Gastroenterology* **122,** 1941–1953
7. Voronina, S., Longbottom, R., Sutton, R., Petersen, O. H., and Tepikin, A. (2002) (2002) *J. Physiol.* **540,** 49–55
8. Mooren, F. Ch., Hlouschek, V., Finkes, T., Turi, S., Weber, I. A., Singh, J., Domschke, W., Schnekenburger, J., Kruger, B., and Lerch, M. M. (2003) *J. Biol. Chem.* **278,** 9361–9369
9. Kasai, H., Li, Y. X., and Miyashita, Y. (1993) *Cell* **74,** 669–677
10. Thorn, P., Lawrie, A. M., Smith, P. M., Gallacher, D. V., and Petersen, O. H. (1993) *Cell* **74,** 661–668
11. Xu, X., Zeng, W., Diaz, J., and Muallem, S. (1996) *J. Biol. Chem.* **271,** 24684–24690
12. Straub, S. V., Giovannucci, D. R., and Yule, D. I. (2000) *J. Gen. Physiol.* **116,** 547–560
13. Kiselyov, K., Shin, D. M., and Muallem, S. (2003) *Cell. Signal.* **15,** 243–253
14. Lee, M. G., Xu, X., Zeng, W., Diaz, J., Wojcikiewicz, R. J., Kuo, T. H., Wuytack, F., Racymaekers, L., and Muallem, S. (1997) *J. Biol. Chem.* **272,** 15765–15770
15. Yule, D. I., Ernst, S. A., Ohnishi, H., and Wojcikiewicz, R. J. (1997) *J. Biol. Chem.* **272,** 9093–9098
16. Li, Q., Luo, X., and Muallem, S. (204) *J. Biol. Chem.* **279,** 27837–27840
17. Pozzan, T., Magalhaes, P., and Rizzuto, R. (2000) *Cell Calcium* **28,** 279–283
18. Tinel, H., Cancela, J. M., Mogami, H., Gerasimenko, J. V., Gerasimenko, O. V., Tepikin, A. V., and Petersen, O. H. (1999) *EMBO J.* **18,** 4999–5008
19. Park, M. K., Ashby, M. C., Erdemli, G., Petersen, O. H., and Tepikin, A. V. (2001) *EMBO J.* **20,** 1863–1874
20. Bruce, J. I., Giovannucci, D. R., Blinder, G., Shuttleworth, T. J., and Yule, D. I. (2004) *J. Biol. Chem.* **279,** 12909–12917
21. Rizzuto, R., Pinton, P., Carrington, W., Fay, F. S., Fogarty, K. E., Lifshitz, L. M., Tuft, R. A., and Pozzan, T. (1998) *Science* **280,** 1763–1766
22. Rizzuto, R., Brini, M., Murgia, M., and Pozzan, T. (1993) *Science* **262,** 744–747
23. Rizzuto, R., Duchen, M. R., and Pozzan, T. (2004) *Science's STKE* http://stke.sciencemag.org/cgi/content/full/sigtrans;2004/215/re1
24. Hoth, M., Fanger, C. M., and Lewis, R. S. (1997) *J. Cell Biol.* **137,** 633–648
25. Gilabert, J. A., and Parekh, A. B. (2000) *EMBO J.* **19,** 6401–6407
26. Pin, C. L., Rukstalis, J. M., Johnson, C., and Konieczny, S. F. (2001) *J. Cell Biol.* **155,** 519–530
27. Pin, C. L., Bonvissuto, A. C., and Konieczny, S. F. (2000) *Anat. Rec.* **259,** 157–167
28. Rukstalis, J. M., Kowalik, A., Zhu, L., Lidington, D., Pin, C. L., and Konieczny, S. F. (2003) *J. Cell Sci.* **116,** 3315–3325
29. Zhu, L., Tran, T., Rukstalis, J. M., Sun, P., Damsz, B., and Konieczny, S. F. (2004) *Mol. Cell. Biol.* **24,** 2673–2681
30. Johnson, C. L., Kowalik, A. S., Rajakumar, N., and Pin, C. L. (2004) *Mech. Dev.* **121,** 261–272
31. Shin, D. M., Zhao, X. S., Zeng, W., Mozhayeva, M., and Muallem, S. (2000) *J. Cell Biol.* **150,** 1101–1112
32. Shin, D. M., Luo, X., Wilkie, T. M., Miller, L. J., Peck, A. B., Humphreys-Beher, M. G., and Muallem, S. (2001) *J. Biol. Chem.* **276,** 44146–44156
33. Luo, X., Popov, S., Bera, A. K., Wilkie, T. M., and Muallem, S. (2001) *Mol. Cell* **7,** 651–660
34. Zhao, X. S., Shin, D. M., Liu, L. H., Shull, G. E., and Muallem, S. (2001) *EMBO J.* **20,** 2680–2689
35. Gupta, N., Rathi, P., and Gupta, R. (2002) *Anal. Biochem.* **311,** 98–99
36. Gildberg, A., and Overbo, K. (1990) *Comp. Biochem. Physiol. B* **97,** 775–7782
37. Deleted in proof
38. Hattori, M., Suzuki, A. Z., Higo, T., Miyauchi, H., Michikawa, T., Nakamura, T., Inoue, T., and Mikoshiba, K. (2004) *J. Biol. Chem.* **279,** 11967–11975
39. Hajnoczky, G., Robb-Gaspers, L. D., Seitz, M. B., and Thomas, A. P. (1995) *Cell* **82,** 415–424
40. Jouaville, L. S., Pinton, P., Bastianutto, C., Rutter, G. A., and Rizzuto R. (1999) *Proc. Natl. Acad. Sci.* **96,** 13807–13812
41. Williams, J. A., Korc, M., and Dormer, R. L. (1978) *Am. J. Physiol.* **235,** 517–524